journal of the mechanical behavior of biomedical materials 155 (2024) 106563

Contents lists available at ScienceDirect

Journal of the Mechanical Behavior of Biomedical Materials

journal homepage: www.elsevier.com/locate/jmbbm

Influence of additives and binder on the physical properties of dental silicate glass-ceramic feedstock for additive manufacturing

Moritz Hoffmann [a,*], Bogna Stawarczyk [a], Jens Günster [b,c], Andrea Zocca [b]

[a] Department of Prosthetic Dentistry, Dental School, University Hospital, LMU Munich, Goethestraße 70, 80336, Munich, Germany
[b] Division 5.4 Advanced Multi-materials Processing, Bundesanstalt für Materialforschung und -prüfung, Unter Den Eichen 87, 12205, Berlin, Germany
[c] Institute of Non-Metallic Materials, Clausthal University of Technology, 38678 Clausthal-Zellerfeld, Germany

ARTICLE INFO

Keywords:
3D-printing
Silicate glass-ceramics
Debinding
Firing

ABSTRACT

Objectives: The aim of the study was to investigate the impact of organic additives (binder, plasticizer, and the cross-linking ink) in the formulation of water-based feedstocks on the properties of a dental feldspathic glass-ceramic material developed for the slurry-based additive manufacturing technology "LSD-print."
Material and methods: Three water-based feldspathic feedstocks were produced to study the effects of polyvinyl alcohol (AC1) and poly (sodium 4-styrenesulfonate) (AC2) as binder systems. A feedstock without organic additives was tested as the control group (CG). Disc-shaped (n = 15) and bar (n = 7) specimens were slip-cast and characterized in the green and fired states. In the green state, density and flexural strength were measured. In the fired state, density, shrinkage, flexural strength (FS), Weibull modulus, fracture toughness (K_{IC}), Martens parameters, and microstructure were analyzed. Disc-shaped and bar specimens were also cut from commercially available CAD/CAM blocks and used as a target reference (TR) for the fired state.
Results: In the green state, CG showed the highest bulk density but the lowest FS, while the highest FS in the green state was achieved with the addition of a cross-linking ink. After firing, no significant differences in density and a similar microstructure were observed for all slip-cast groups, indicating that almost complete densification could be achieved. The CAD/CAM specimens showed the highest mean FS, Weibull modulus, and K_{IC}, with significant differences between some of the slip-cast groups.
Significance: These results suggest that the investigated feedstocks are promising candidates for the slurry-based additive manufacturing of restorations meeting the class 1a requirements according to DIN EN ISO 6871:2019–01.

1. Introduction

All-ceramic fixed dental prostheses (FDPs) are characterized by high biocompatibility, outstanding esthetic appearance (Albakry et al., 2003; Conrad et al., 2007; Kelly et al., 1996; Sadowsky, 2006), low thermal conductivity, and minimal plaque accumulation (Conrad et al., 2007; Kelly et al., 1996; Sadowsky, 2006). Dental feldspathic glass-ceramics are mainly used for crowns, veneers, inlays, and onlays, and the mechanical properties are considered too low for multiunit FDPs (Bajraktarova-Valjakova et al., 2018; Kelly and Benetti, 2011). Feldspathic glass-ceramics can be processed in different ways to manufacture FDPs. Conventionally, they can be layered or pressed from pellets. However, computer-aided design/manufacturing (CAD/CAM) workflows for milling (subtractive manufacturing) from a block are becoming increasingly popular owing to their simplicity and time savings (Turkyilmaz et al., 2021). Recently, interest has also been shown in different additive manufacturing (AM) technologies using different ceramic types to manufacture FDPs (Galante et al., 2019; Ioannidis et al., 2020; Lerner et al., 2021; Unkovskiy et al., 2022; Wang and Sun, 2021; Wang et al., 2019; Rodrigues et al., 2020), including for improving esthetics by, e.g., fabricating ultrathin and nonpreparation veneers (Unkovskiy et al., 2022).

However, technologies associated with VAT polymerization, particularly stereolithography (SLA) and digital light processing (DLP), appear promising for the fabrication of dental objects due to their high accuracy and resolution. Although material jetting (MJ) and robocasting (RC) have also shown interesting results, objects produced by these technologies typically exhibit lower resolution/accuracy and inferior

* Corresponding author. Department of Prosthetic Dentistry, University Hospital, LMU Munich, Goethestrasse 70, 80336, Munich, Germany.
E-mail address: moritz.hoffmann@med.uni-muenchen.de (M. Hoffmann).

https://doi.org/10.1016/j.jmbbm.2024.106563
Received 15 February 2024; Received in revised form 23 April 2024; Accepted 23 April 2024
Available online 25 April 2024

mechanical properties compared to SLA and DLP, limiting their applicability for restorative purposes (Branco et al., 2023). Compared with subtractive manufacturing, AM has the potential to reduce manufacturing costs and material waste (Barazanchi et al., 2017; Daher et al., 2022). One of the main challenges to the commercial adoption of AM for dental ceramics is the long processing time compared with CAD/CAM milling. AM fabrication and thermal postprocesses typically amount to tens of hours up to several days (Lüchtenborg et al., 2022), whereas milling and firing a ceramic FDP can be completed in less than 1 h (Park et al., 2020).

The layerwise slurry deposition (LSD-print) technology is a promising AM approach to accelerating production. As with most AM techniques, the LSD-print process takes place in a layer-by-layer fashion and offers high geometric freedom for the manufacturing of complex components. According to ISO/ASTM 52900:2022–03 LSD-print is classified in the category of binder jetting (BJ) and can be considered a variation of slurry-based BJ (Cima et al., 2001). Similar to BJ, ink is selectively printed into powder layers by means of an inkjet printhead to locally bind the powder particles and define the cross-section of the object to be built. However, in contrast with BJ, in the LSD-print process, a water-based ceramic suspension (slurry) is used as feedstock instead of a dry powder. The feedstock is deposited by means of a doctor blade to form a thin layer in the wet state, which is then carefully dried prior to printing the ink. The use of a liquid feedstock allows the use of finer ceramic particles compared with dry powders, where powder flowability and agglomeration become issues for small particle sizes (typically <10 μm (Tomas and Kleinschmidt, 2009)). Furthermore, the drying shrinkage of the wet layers, which is driven by capillary forces, leads to high packing of the particles up to a relative packing density of >60% (Zocca et al., 2017). The result of stacking these layers is a highly packed powder bed, in which the printed part is inscribed. At the end of the process, the printed part ("green body" in ceramic terminology) can be washed out of the surrounding powder, dried, debinded to burn out the organic additives, and finally fired in a high-temperature furnace.

In recent years, the LSD-print process (Fig. 1) has been used for several ceramic materials, including traditional silicate ceramics (porcelain (Lima et al., 2018),) and technical ceramics (alumina (Zocca et al., 2017), and SiSiC (Zocca et al., 2019)).

However, for dental applications, challenges are posed by the strict requirements of manufacturing tolerances, surface quality, and mechanical and esthetic properties (Galante et al., 2019). The formulation of the slurry feedstock is one of the most important steps in optimizing the LSD-print process to satisfy these requirements. Investigations into the drying of granular ceramic films have shown that wet ceramic layers crack during drying if the drying stress is higher than the fracture resistance of the layer (Chiu et al., 1993). Because the drying stress is inversely proportional to the mean particle size of the slurry (Chiu et al., 1993), the drying of ceramics with fine particle sizes is challenging and often necessitates a careful selection of additives to increase the fracture resistance and flexibility of the layer (Hotza and Greil, 1995). Contrary to traditional silicate ceramics, raw materials for dental silicate ceramics consist almost exclusively of a fine particle size fraction (<5 μm) and do not contain minerals such as clay minerals, which impart plasticity to the suspension. To finely disperse the particles and avoid cracking during drying of the layers in the LSD-print process, the use of additives in the slurry formulation is a necessity in most cases. Organic additives are preferred for dental applications because they can be eliminated during thermal postprocessing. However, it is essential to ensure that the selected additives do not negatively affect the final material properties of dental ceramics. Especially, the formation of cracks and large pores during the process and debinding must be avoided. Ceramic processing additives can be broadly categorized into two groups (Carter and Norton, 2007): dispersants (deflocculants) used to achieve a homogeneous and stable dispersion of the ceramic particles in the liquid medium; and binders and plasticizers. Binders are usually high molecular weight polymers that impart green strength to the layers and green body, important to avoid cracking and facilitate handling. Plasticizers are usually lower molecular weight polymers that can be added to increase plasticity and decrease brittleness (Carter and Norton, 2007).

The ink that is selectively printed to consolidate the powder layers is another additive used in LSD-print technology and in BJ. Similar to other organic additives, the ink needs to be eliminated during thermal postprocessing, making it essential to understand its effect on the green and fired parts. The so-called "ink" is usually named "binder" in binder

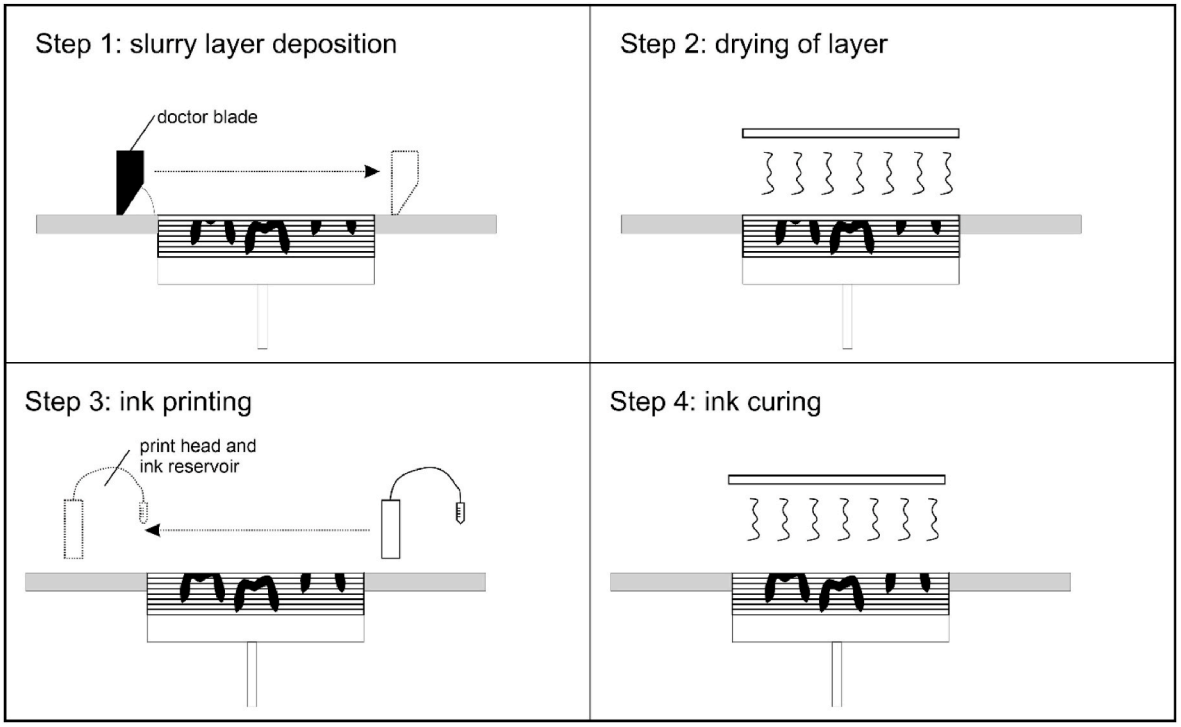

Fig. 1. Depiction of the LSD-print process.

jetting technology, but this terminology will not be used in this report to avoid inconsistencies with the term "binder" as commonly used in ceramic processing. Specifically, in this investigation, the ink was a liquid resin that is thermally cross-linked to impart stability to the green part. A recent investigation proposed and validated that slip-cast specimens can be used to estimate the properties of as-printed (i.e., green) specimens produced by LSD-print technology (Diener et al., 2023). It was also shown that if the ink was mixed in the feedstock, the density and flexural strength of slip-cast green bodies were comparable with those of the as-printed specimens with the same concentration of ink. In the current investigation, a similar approach was implemented to analyze the effect of three different feedstock formulations and of the ink on the properties of slip-cast specimens. Feedstock with additive composition 1 (AC1) contained polyvinyl alcohol (PVA) as a binder, while feedstock with AC2 contained poly(sodium 4-styrolsulfonate) (PSS) as a binder and polyethylene glycol (PEG200) as a plasticizer. A feedstock without additives was used as the control (CG). Furthermore, the slip-cast specimens were compared after firing with a commercial target reference (TR) consisting of specimens sectioned from CAD/CAM blocks of the same nominal material composition.

The null hypotheses tested were: 1) the formulation of feedstocks AC1 and AC2 has no effect on the material properties of slip-cast specimens compared with CG. The density and biaxial flexural strength (FS) of both the green and fired states were compared. Shrinkage, fracture toughness (K_{1C}), and Martens parameters (HM and E_{IT}) were compared in the fired state; 2) the addition of ink to feedstocks AC1, AC2, and CG has no effect on the material properties of slip-cast specimens. The density and FS were compared in both the green and fired states. Shrinkage, K_{1C}, and Martens parameters were compared in the fired state; and 3) in the fired state, the specimens produced with AC1 and AC2 feedstocks do not have different material properties compared with those produced with TR. The density, FS, K_{1C}, and Martens parameters were compared.

2. Materials and methods

Fig. 2 provides an overview of the study design and characterization methods.

2.1. Fabrication and characterization of feedstocks

The powder used to fabricate the slurry feedstock was feldspathic silicate powder (FSP). The particle size distribution of the raw powder material was measured by using the laser diffraction method (Mastersizer 3000, Malvern Panalytical, Malvern, UK). The powder was dispersed in water containing 3 mmol/l $Na_4P_2O_7$, and the particle size distribution was determined according to ISO 13320:2020–01. The feedstocks were prepared as shown in Table 1.

First, the binder was dissolved in deionized water on a magnetic stirrer plate (20 °C, 2 h), followed by sonication for 10 min and the addition of the other components. Finally, the feedstock was mixed in PVC bottles on a roller mixer for 24 h with a drop of octanol to reduce foam formation.

The rheology of the slurries was characterized by measuring a shear-controlled flow curve with linear shear ramps from 10 to 500 s^{-1} and a shear rate of 500 to 10 s^{-1}. The measurements were performed with a plate-plate (∅:25 mm) configuration in a rotational rheometer (Anton Paar MCR301, Graz, Austria) at 25 °C.

2.2. Specimen fabrication

For the slip-casting molds (disc and bar), a standardized self-constructed form was designed (Rhino 7, Robert McNeel & Associates, Seattle, USA) and milled using a 5-axis milling machine (Acura 65, Hedelius, Meppen, Germany). The form was molded in silicone (Adisil rose, Siladent, Goslar, Germany) and cast in gypsum (pico-crema soft, picodent, Wipperfürth, Germany).

Different feedstock compositions (Table 1), with or without ink, were used to slip cast discs and bars. Commercially available CAD/CAM blocks (VITABLOCS Mark II, VITA Zahnfabrik, Bad Säckingen, Germany) were used for TR. Therefore, cylinders were milled with a 5-axis milling machine (Ceramill Motion 2, Amann Girrbach, Koblach, Austria), and discs (n = 15) were cut. The bar specimens (n = 7) were cut horizontally to the longitudinal axis directly from the CAD/CAM blocks. A precision cutting machine (Secotom 50, Struers, Ballerup, Denmark) with a diamond cutting disc (0.02 mm/min, 3500, and M1D13, Struers) was used under water cooling.

Before casting, the feedstocks were mixed for an additional 72 h using a tube roller. For the specimens produced with ink, ink was added to the feedstock and mixed for 30 min (RH basic 2, IKA-Werke, Staufen, Germany). All groups were degassed for 120 s at 100 mbar (Epovac, Struers) to eliminate air pockets. The specimens remained in the gypsum mold until they dried. Excess material on the upper surface of the mold was gently removed using a razor blade. The specimens with ink were thermally cross-linked at 130 °C for 12 h (Secatherm, BEGO, Bremen, Germany). The specimens were positioned on a firing tray covered with quartz powder and fired in a ceramic furnace; specimens including ink were processed with a two-stage heat treatment for debinding and firing

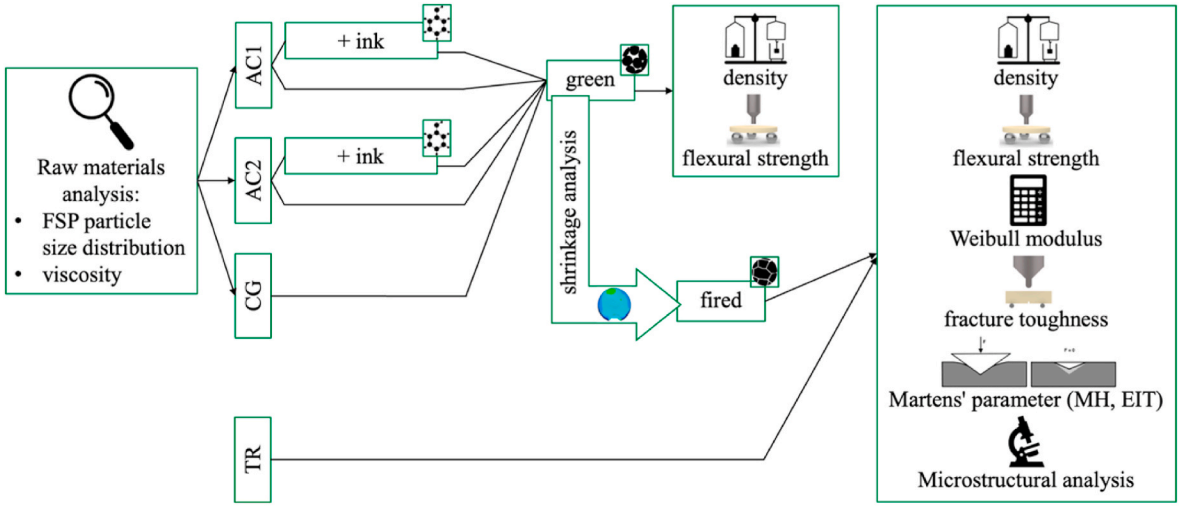

Fig. 2. Study design.

Table 1
Used products sorted by name, specification, manufacturer, LOT No. and composition of slurry feedstocks AC1, AC2, and CG.

	Composition	Manufacturer	Lot No./CAS No.	Feedstock composions				
				Feedstock AC1 [wt%]		Feedstock AC2 [wt%]		Feedstock CG [wt%]
				–	with ink	–	with ink	
FSP	Experimental composition of silicate feldspar powder	VITA Zahnfabrik GmbH, Bad Säckingen, Germany	–	67.65	62.06	65.30	60.03	66.67
H_2O	H_2O, deionized			31.00	28.44	32.70	30.01	33.33
PVA (POVAL 18–88)	Polyvinyl alcohol 18-88	Kuraray Europe GmbH, Hattersheim am Main, Germany	N120125032	0.85	0.78	–		–
PSS	Poly(sodium 4-styrolsulfonate)	SIGMA-ALDRICH Corp., St. Louis, USA	MKBB3350	–		1.00	0.96	–
DolaPix CE64	Synthetic polyelectrolyte, ammonium salt of polyacrylic acid.	Zschimmer und Schwarz Chemie GmbH, Lahnstein, Germany	228341001	0.50	0.45	0.50	0.42	–
PEG 200	Polyethylene glycol 200	SIGMA-ALDRICH Corp., St. Louis, USA	BCCF0271	–		0.50	0.42	–
PDB Binder Typ A (ink)	Phenolic binder	voxeljet AG, Friedberg, Germany	–		8.27		8.16	–
VITABLOCS Mark II 3M2C (TR)	SiO_2: 56–64 wt%, Al_2O_3: 20–23 wt%, Na_2O: 6–9 wt%, K_2O: 6–8 wt%, CaO: 0.3–0.6 wt%	VITA Zahnfabrik GmbH, Bad Säckingen, Germany	194410	–		–		–

Table 2
Debinding and firing parameters.

	T_{start} (°C) on–>	heating rate (K/min)	T_{end1} (°C)	$t_{holding}$ (min)	cooling rate (K/min)	T_{end2} (°C	vacuum (°C/%/min
Debinding	200	5	550	–	–	–	–
Firing	550	45	1190	15	55	600	1190/100/12

(Table 2; AUSTROMAT 654, DEKEMA, Freilassing, Germany).

The discs for biaxial flexural strength measurements were ground to a final height of 1.2 ± 0.2 mm (3 μm; ∅: 12 mm, DIN EN ISO 6872:2019–01), and the bars to final dimensions of 4 × 3 × 15 ± 0.2 mm. For single edge V-notched beam fracture toughness (SEVNB, DIN EN ISO 6872:2019–01), 7 bars were placed one after the other on the narrow side in a custom specimen holder and fixed (Futar D Fast, Kettenbach, Eschenburg, Germany). A prenotch (depth: 600–700 μm, width: 450 μm) was cut at the center of each bar perpendicular to its longitudinal axis using a precision cutting machine (Secotom 50, Struers) and a diamond cutting disc (0.02 mm/min, 3500 rpm; M1D13, Struers) under water cooling. For final notch (depth: 0.8–1.2 mm), the specimen holder was transferred to a notching machine (MTD 500+, SD Mechatronik, Feldkirchen-Westerham, Germany), and an industrial blade (37040, MARTOR, Solingen, Germany) lubricated with polishing paste (3 μm; 9300, Komet Dental Gebr. Brasseler, Lemgo, Germany) was loaded with 600 g and moved 1500 to 2500 times. Notch depth was measured by using a digital microscope (VHX 970F, Keyence, Osaka, Japan). All specimens were cleaned in 96% ethanol (Otto Fischar, Saarbrücken, Germany) for 3 min in an ultrasonic bath (DT 31 H, BANDELIN, Berlin, Germany).

2.3. Density measurement and microstructure

The density was determined in the green (n = 4) and fired states (n = 4). The green-state specimens were stored in an incubator with silica gel at 37 °C (BE 500, Memmert, Schwabach, Germany). When their weight was constant (New Classic MS, METTLER TOLEDO, Columbus, USA), the diameter and height were measured with calipers (9M05.3.01, Hogetex, Nieder-Olm, Germany), and the geometric bulk density was calculated.

The bulk density of the fired specimens was determined using the Archimedes method following ISO 18754:2020–04 in deionized water:

$$\rho_b = \frac{m_1}{m_3 - m_2} \bullet \rho_1 \quad (1)$$

where ρ_b is the bulk density, m_1 is the mass of the dry test specimen, m_2 is the mass of the immersed specimen, and m_3 is the mass of the soaked specimen.

The absolute density of the material was measured by helium pycnometry (Pycnomatic ATC, Porotec, Waldems, Germany), and the values were used to calculate the relative density from the ratio of the bulk density to the absolute density.

One specimen from each group was embedded in resin (Epofix resin and hardener, Struers, Denmark) and prepared for microscopic investigation. A polished surface was obtained on a grinding and polishing machine (Tegramin-30, Struers) in successive steps from 500 to 1200 grade grinding surface, followed by 9-μm, 3-μm, 1-μm, and 0.25-μm diamond suspension polishing.

The polished surface was observed under a Keyence 7000 digital microscope with coaxial illumination at increasing magnifications. The embedded specimens were etched for 12 s with a 5% HF solution before scanning electron microscopy (SEM) analysis. The specimens were carbon coated in a sputtering chamber (CED 030, Baltec AG, Switzerland) and analyzed using a LEO Gemini 1530 VP SEM (Zeiss, Germany) mounting an EDX System XFlash Detector 5030 with software Esprit 1.9 (Bruker, Germany). The SEM images were recorded using a four-quadrant backscattered electron detector (BSD signal) at 15 kV. The etched area fraction was estimated using image analysis (ImageJ software) of five different SEM images.

2.4. Shrinkage measurement

Shrinkage was determined using an analysis software program (QualityCheck, r2 dei ex machina, Remchingen, Germany) with standardized dimensions of green state specimens (n = 15). Fired discs were coated (Arti-Spray, Dr. Jean Bausch, Cologne, Germany) and scanned (6 μm, Ceramill Map 400, Amann Girrbach AG). The generated STL-Data were imported into the analysis software program, and the volume shrinkage was determined automatically.

2.5. Flexural strength measurement

The biaxial flexural strength was determined in the green and fired states by using a piston-on-three-ball setup (n = 15). Steel balls (∅: 3.2 mm) were arranged to form an equidistant triangle on a metal platform. The specimens were positioned concentrically between the piston (∅: 1.6 mm) and the support circle (∅: 10.2 mm). The load was centrally applied using a universal testing machine (1 mm/min; 1445, Zwick/Roell) until fracture. For calculating the flexural strength, the fracture load was recorded, and the following formula used (DIN EN ISO 6872:2019–01):

$$\sigma = \frac{-0.2387P(X-Y)}{d^2} \tag{2}$$

where σ: flexural strength (MPa); P: fracture load (N); d: thickness (mm). X and Y as coefficients were calculated as follows:

$$X = (1+\upsilon) ln \left(\frac{r2}{r3}\right)^2 + \frac{1-\upsilon}{2} \bullet \left(\frac{r2}{r3}\right)^2 \tag{3}$$

$$Y = (1+\upsilon)\left[1 + ln\left(\frac{r1}{r3}\right)^2\right] + (1-\upsilon) \bullet \left(\frac{r1}{r3}\right)^2 \tag{4}$$

where υ: Poisson ratio; r1: radius of the support circle (mm); r2: radius of the piston (mm); r3: radius of the specimen (mm)

For calculating the X and Y coefficients, knowledge of the Poisson ratio is necessary. For fired specimens, a value of $\upsilon = 0.18$ was selected as measured for VITABLOCS Mark II (TR) by Coldea et al. (2015). As the Poisson ratio of the green specimens was unknown and could not be measured accurately, it was estimated as $\upsilon = 0.2$ (Greaves et al., 2011).

2.6. Fracture toughness measurement

The fracture toughness was measured using a three-point bending test setup (n = 7). The specimens were stored at 100 °C for 24 h (BE 500, Memmert, Schwabach, Germany). The beams were positioned with the notched surface downward on the bearings (distance: 10 mm). The notches were filled with silicone oil (BALLISTOL, Aham, Germany). The load was centrally applied using a universal testing machine (0.5 mm/min; 1445, Zwick/Roell) until fracture. The relative notch depth was measured using a digital microscope (VHX 970F, Keyence). For calculating the fracture toughness, the fracture load was recorded, and the following formula used (DIN EN ISO 6872:2019–01):

$$K_{1C} = \frac{F}{b\sqrt{w}} \bullet \frac{S}{w} \bullet \frac{3\sqrt{\alpha}}{2(1-\alpha)^{1.5}} Y \tag{5}$$

where K_{1C}: fracture toughness (MPa $\sqrt{m}$); F: fracture load (MN); b: width (m); w: height (m); S: bearing span (m); α: relative depth of the notch (m). Y as coefficient for the span to height ratio was calculated as follows:

$$Y = 1.9109 - 5.1552\alpha + 12.6880\alpha^2 - 19.5736\alpha^3 + 15.9377\alpha^4 - 5.1454\alpha^5 \tag{6}$$

2.7. Martens parameter

Martens hardness (HM) and indentation modulus (E_{IT}) were determined using a Martens hardness testing machine (ZHU 0.2, Zwick/Roell) (n = 7). The beams were loaded on their wide side with 9.81 N for 10 s using a Vickers diamond indenter (α = 136°). HM and E_{IT} were calculated within the testing software program (testX-pertV12.3, Master, Zwick/Roell) using the following formulas (DIN EN ISO 14577–1:2015):

$$HM = \frac{F}{A_s(h)} \tag{7}$$

where: HM: Martens hardness (N/mm^2); F: applied loading (N); A_s(h): penetrated area of indenter at distance h from tip to specimen surface (mm^2).

$$E_{IT} = \left(1-\upsilon_S^2\right)\left(\left(2\sqrt{\frac{A_P(h_C)}{\sqrt{\pi}S}}\right) - \left(\frac{1-\upsilon_i^2}{E_i}\right)\right)^{-1} \tag{8}$$

where E_{IT}: elastic indentation modulus (N/mm^2); $A_p(h_c)$: projected contact area at loading (mm^2); υ: Poisson ratio of specimen and indenter with $\upsilon_S = 0.18$ (Coldea et al., 2015) and $\upsilon_I = 0.3$; S: contact stiffness derived from force removal curve.

2.8. Statistical analysis

Descriptive statistics were calculated, followed by the Kolmogorov-Smirnov-test to detect deviations from a normal distribution. Univariate ANOVA with partial eta-squared (η_p^2) was performed to determine the influence of the feedstock and additive composition. The impact of the separate parameters was analyzed by using one-way ANOVA with the post hoc Scheffé test or independent *t*-test. Parameters deviating from the normal distribution were evaluated by using the Kruskal-Wallis test followed by the Mann-Whitney *U* test. Statistical analysis was performed using SPSS statistics (V 27.0, IBM Corp, Armonk, USA; α = 0.05). The Weibull modulus was calculated using the maximum likelihood method and a 95% confidence interval (Butikofer et al., 2015). The fracture types of the flexural strength specimens were classified, and the relative frequencies with 95% confidence intervals were calculated by using the Ciba Geigy Table.

3. Results

Density, FS, HM, E_{IT}, and K_{1C} showed no deviation from normal distribution; therefore, parametric tests were used for data analysis. In contrast, shrinkage deviated from a normal distribution, and nonparametric tests were used for this analysis (Table 3).

3.1. Feedstock characterization

The powder particle size distribution percentiles by volume were calculated as d(v,10) = 1.98 μm, d(v,50) = 5.80 μm, d(v, 90) = 14.90 μm, and d(v,97) = 21.50 μm (Fig. 3, A). Fig. 3, B shows the rheological flow curves of the slurry feedstocks AC1, AC2, and CG.

CG had the lowest viscosity and showed shear thickening behavior at shear rates >100 s^{-1}. AC1 and AC2 had considerably higher (approx. 1 order of magnitude) viscosity than CG and showed a pronounced shear thickening (dilatant) behavior. AC1 had a lower viscosity than AC2 at low shear rates, but both slurries had similar viscosities at shear rates >300 s^{-1}. The waviness of the AC1 curve at shear rates >350 s^{-1} was due to artifacts in the measurement related to partial drying and coagulation of the suspension.

3.2. Density and microstructure

All feedstock compositions, with or without ink usage, showed higher bulk density in the fired state than in the green state ($p < 0.001$) (Table 3).

In the green state, CG resulted in the highest bulk density, followed by AC1 and AC1+ink ($p < 0.001$ to 0.013). AC2+ink showed lower bulk density than CG, AC1, and AC1+ink ($p < 0.001$ to 0.029) (Table 3).

In the fired state, CG was in same value range as AC1 ($p = 0.688$) and resulted in a higher bulk density than AC1+ink, AC2, and AC2+ink ($p < 0.001$ to 0.048). The use of AC2+ink resulted in the lowest bulk density

Table 3
Descriptive statistics showing the mean and standard deviation of bulk density, absolute density, relative density, flexural strength, Weibull modulus, fracture toughness, Martens hardness, and indentation modulus depending on the groups.

			Bulk density [g/cm^3] Mean ± SD	Absolute density [g/cm^3] Mean ± SD	Relative density [%]	Flexural strength [MPa] Mean ± SD	Weibull modulus (95%CI)	Fracture toughness [MPa^{a}m$^{0.5}$]	Martens hardness [MPa]	Indentation modulus [GPa]
AC1	ink	green	1.44 ± 0.02$^{bc\ I}$	–	–	8.53 ± 2.95^{aBI}	–	–	–	–
		fired	2.39 ± <0.01^{bIIy}	2.41 ± <0.01^{aAx}	99.2	90.8 ± 4.6^{aAIIyz}	23(12; 40)	1.05 ± 0.07^{bBy}	3379 ± 183^{ax}	55.6 ± 2.8^{ax}
	–	green	1.46 ± 0.03^{bcI}	–	–	0.41 ± 0.27^{abAI}	–	–	–	–
		fired	2.40 ± <0.01^{bcIIy}	2.41 ± <0.01^{aAx}	99.6	87.8 ± 5.8^{aAIIyz}	18(9; 31)	1.13 ± 0.08^{bAyz}	3422 ± 237^{ax}	56.7 ± 4.5^{ax}
AC2	ink	green	1.34 ± 0.04^{aI}	–	–	4.91 ± 0.75^{bBI}	–	–	–	–
		fired	2.39 ± <0.01^{aIIy}	2.41 ± <0.01^{aAx}	99.2	92.0 ± 5.4^{aBIIz}	19(10; 33)	0.86 ± 0.06^{aBx}	3463 ± 88a^{ax}	57.1 ± 1.7^{aax}
	–	green	1.39 ± 0.03^{abI}	–	–	0.28 ± 0.11^{bAI}	–	–	–	–
		fired	2.38 ± <0.01^{bIIy}	2.40 ± <0.01a^{Ax}	99.2	83.6 ± 8.9^{aAIIy}	11(5; 19)	1.02 ± 0.09^{aAxy}	3449 ± 143^{ax}	57.1 ± 2.4^{ax}
CG	–	green	1.50 ± 0.01^{cI}	–	–	0^{aI}	–	–	–	–
	–	fired	2.40 ± <0.01^{cIIy}	2.41 ± <0.01^{ax}	99.6	88.4 ± 6.1^{aIIyz}	16.(8; 28)	1.12 ± 0.08^{abyz}	3381 ± 165^{ax}	55.2 ± 2.6^{ax}
TR	–	–	2.43 ± <0.01^{dz}	2.45 ± <0.01^{y}	99.2	93.8 ± 4.7^{z}	24(13; 41)	1.25 ± 0.10^{z}	3640 ± 74^{x}	59.5 ± 1.7^{x}

^{abcd} different letters indicate significant differences between the feedstock within the factor ink usage and one state.
^{AB} different letters indicate significant differences between the factor ink usage within one feedstock and state.
$^{I\ II}$ different numbers indicate significant differences between the state within one feedstock and the factor ink usage.
^{xyz} different letters indicate significant differences between fired and TR.
^{a} indicates deviation from a normal distribution.

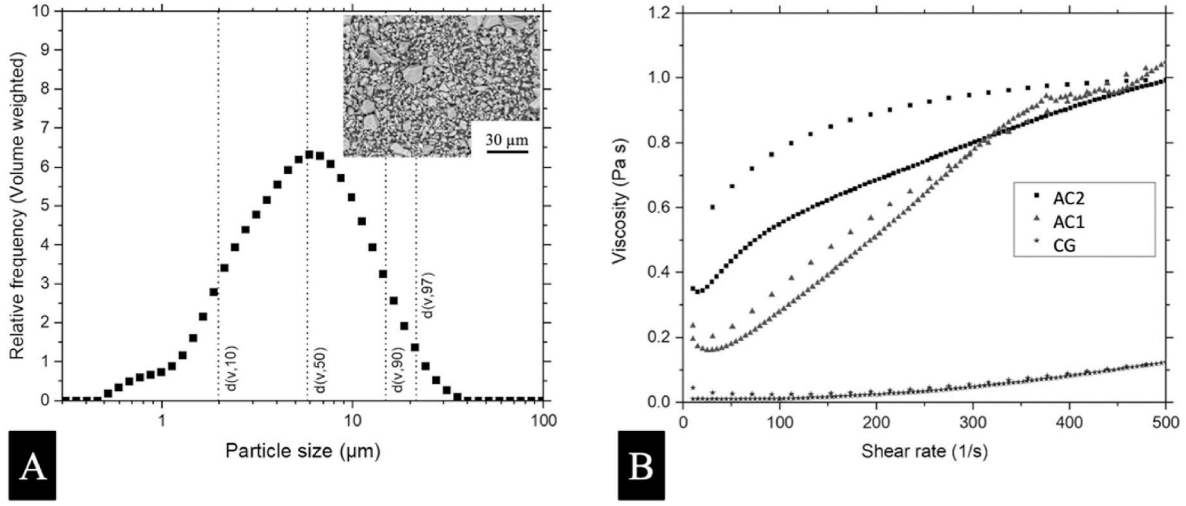

Fig. 3. Particle size distribution and SEM image of the FPS powder (A) and rheological flow curves of slurry feedstocks AC1, AC2, and FPS + H2O. Points with larger spacing indicate a return curve (decreasing shear rate) (B).

of all the groups in the fired state ($p < 0.001$ to 0.023). TR showed a higher density than all slip-cast fired specimens ($p < 0.001$) and had higher absolute density compared with all slip-cast groups ($p < 0.001$). However, the relative density of slip-cast fired groups was equal to that of TR or higher (Table 3).

All slip-cast fired specimens were found to have similar microstructures Fig. 4 shows a microstructural comparison between all groups. However, clear microstructural differences were observed between the slip-cast and TR specimens.

As representative microstructures for the slip-cast fired specimens AC2+ink will be compared in more detail to TR. Low magnification optical microscope images of the polished surfaces revealed an almost fully dense microstructure in both AC2 + ink (Fig. 4A) and TR (Fig. 4D), with few irregularly distributed round pores. Slightly larger defects were observed in AC2 + ink (e.g., the largest round pore in Fig. 4A has ∅: ca. 35 µm) compared with TR (e.g. the largest round pore in Fig. 4D has ∅: ca. 25 µm). Higher magnification (Fig. 4B–E) showed a fine distribution of crystals (bright areas) in a glassy matrix (darker background). The SEM images (Fig. 4C–F) of the etched surface reveal different dissolution rates of the phases, leaving large pores that were visible as black areas in the SEM images. The etched areas estimated by image analysis were 26.4 ± 0.4% for TR and 21.6 ± 1.1% for AC2+ink. SEM and energy-dispersive X-ray spectroscopy (EDX) analyses (Fig. 5) confirmed the presence of at least two distinct crystal phases, one richer (Fig. 5, B) and one poorer (Fig. 5, C) in aluminum and sodium, respectively.

3.3. Shrinkage

The use of feedstock AC1 resulted in the same range of shrinkage as AC2+ink and showed higher volume shrinkage than AC1+ink, AC2, and CG ($p < 0.001$–0.008) (Fig. 6). The CG resulted in the lowest volume shrinkage ($p < 0.001$). The use of ink decreased the volume shrinkage of AC1+ink ($p = 0.008$) and increased that of AC2+ink ($p = 0.036$).

3.4. Flexural strength

The results of the flexural strength measurements are reported in Table 3, and the relative frequencies of the fracture types are presented in Fig. 7.

The firing state ($\eta_p^2 = 0.989$, $p < 0.001$) had the highest impact on FS (Table 3), followed by ink usage ($\eta_p^2 = 0.284$, $p < 0.001$), and an

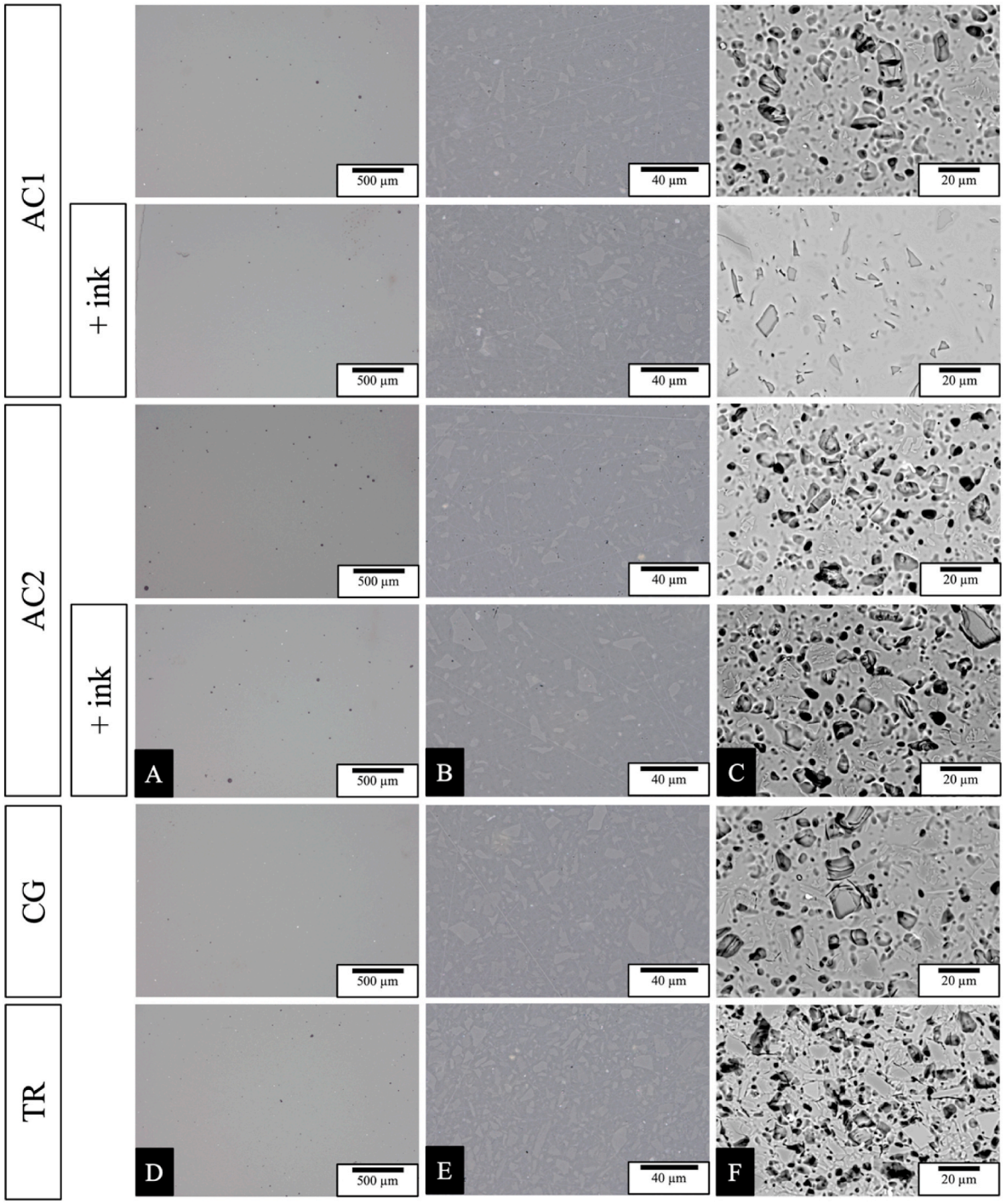

Fig. 4. Microstructure analysis: Optical microscopy of polished surface (left and center column) and SEM images of etched surface (right column).

interaction between feedstock composition, ink usage, and firing state ($\eta_p^2 = 0.047$, $p = 0.010$) (Table 3).

In the green state, the usage of ink increased FS by approximately 20 times, resulting in the highest FS for AC1+ink ($p < 0.001$), followed by AC2+ink ($p < 0.001$). The green strength of the CG could not be measured because of the low mechanical strength of the specimens.

Within the feedstocks in the fired state, the use of AC2+ink showed a higher FS than AC2 ($p = 0.025$). Every other pairwise comparison was not significant ($p \geq 0.088$). TR showed a higher FS than AC2 ($p = 0.003$). Every other pairwise comparison was not significant ($p \geq 0.088$).

Weibull modulus differences were observed where AC2 showed a lower Weibull modulus ($m = 10.7$) than TR ($m = 23.8$) and AC1+ink ($m = 23.2$) (Table 3).

3.5. Fracture toughness

The fracture toughness of AC1 and AC2 was in the same range as CG when no ink was used ($p = 0.419$ to 0.999); however, the addition of ink led to a significant decrease in fracture toughness (AC1: $p = 0.049$, AC2: $p = 0.003$) (Table 3).

TR showed higher fracture toughness than AC1+ink, AC2, and AC2+ink ($p < 0.001$ to 0.005), but no significant differences with AC1 and CG (Table 3).

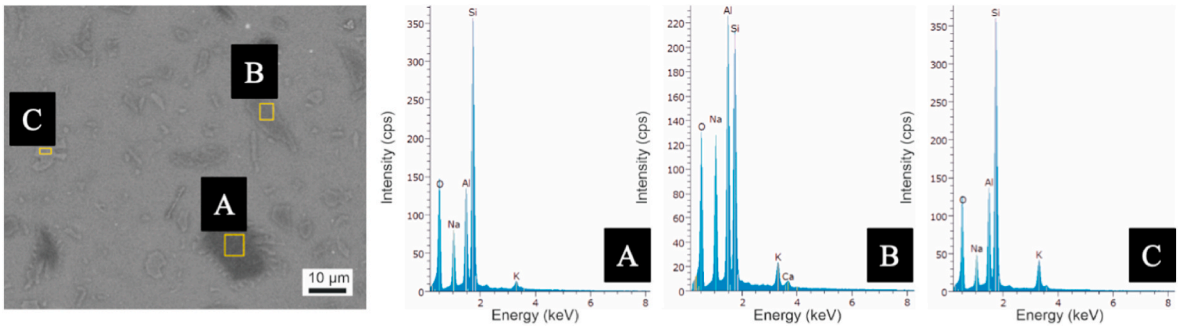

Fig. 5. SEM image of the microstructure and the corresponding EDX patterns.

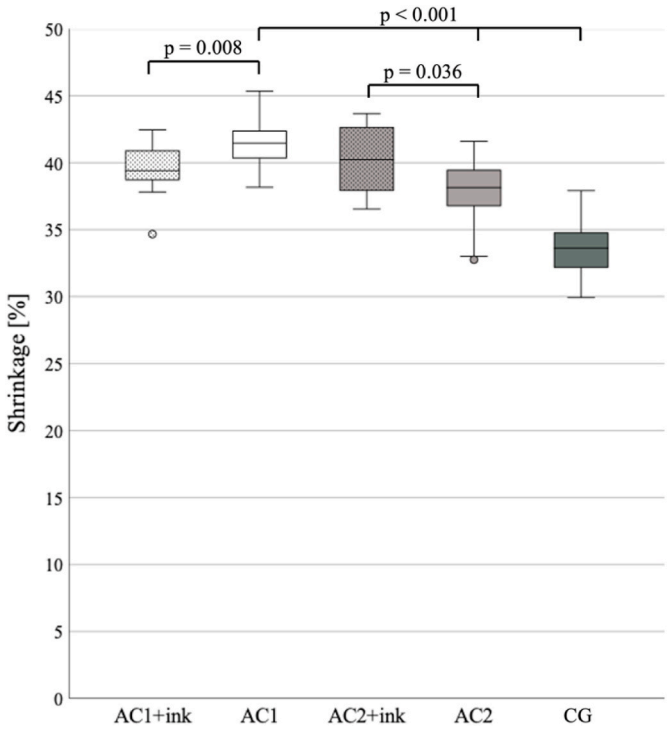

Fig. 6. Boxplots of all tested groups for volume shrinkage, including an outlier within the AC1+ink and AC2 groups.

3.6. Martens parameter

No significant impact of feedstock composition (HM: $p = 0.506$; EIT: $p = 0.267$) or ink usage (HM: $p = 0.810$; EIT: $p = 0.568$) on MH and EIT was observed, and all specimens produced by slurry feedstock and TR were in the same range ($p = 0.267$ to 0.506) (Table 3).

4. Discussion

The aim of the present investigation was to analyze the effect of organic additives for ceramic-based slurry feedstocks paired with the addition of an ink on the material properties of slip-cast specimens. The material properties of interest were the density, FS, shrinkage, K_{IC}, HM, and E_{IT}. Based on this objective, the null hypotheses tested were: 1) the formulation of feedstocks AC1 and AC2 has no effect on the material properties of slip-cast specimens compared with CG. The density and biaxial flexural strength (FS) of both the green and fired states were compared. Shrinkage, fracture toughness (K_{1C}), and Martens parameters (HM and E_{IT}) were compared in the fired state; 2) the addition of ink to feedstocks AC1, AC2, and CG has no effect on the material properties of slip-cast specimens. The density and FS were compared in both the green and fired states. Shrinkage, K_{1C}, and Martens parameters were compared in the fired state; and 3) in the fired state, the specimens produced with AC1 and AC2 feedstocks do not have different material properties compared with TR. The density, FS, K_{1C}, and Martens parameters were compared.

Significant effects were found; thus, all three null hypotheses were rejected for at least one of the evaluated groups.

4.1. Discussion of null hypothesis (1): influence of state and additives

CG achieved the highest green density, and the use of additives led to a significant decrease in green density. This decrease can be explained by the increase in viscosity and steric hindrance caused by the addition of the binder and plasticizer, which hindered the rearrangement of particles forming the cast, thus reducing the packing density (Hampton et al., 1988).

The use of additives in AC1 and AC2, however, had a positive effect on the green strength compared with the CG. Although the addition of binder and plasticizer decreases the packing density in slip-cast specimens, specimens of the control group made from a slurry feedstock without additives were so mechanically unstable that a measurement of FS was not possible. However, the use of additives provided sufficient stability to handle the specimens in the green state. The strength of the green body is governed by either the polymer's cohesive strength (fracture in the polymer) or the adhesion forces at the polymer–ceramic surface (fracture along the interface) (Uhland et al., 2001). PVA has been reported to have both high cohesive and adhesive strength, associated with the interaction of hydroxyl groups pendant from its carbon backbone with the hydrophilic surface of the ceramic particles (Kim et al., 2005). The high strength was confirmed in the current study, in which AC1 with PVA as a binder resulted in the highest green strength. From the perspective of the application of feedstocks in the LSD-print process, the use of feedstock without binders (CG) led to very weak green bodies, which correspond to weak powder layers prone to the formation of defects in the additive manufacturing process. Therefore, these results highlight the importance of using appropriate additives in the feedstock composition.

In the fired state, the shrinkage values were the only differences observed between the groups. A negative effect of the additives in AC1 and AC2 on the debinding and firing processes can therefore be excluded. Despite small variations in green density, the specimens of all groups reached almost full densification (>99% relative density, confirmed by microstructural analysis) after firing. It follows that the shrinkage must be lowest for the specimens with the highest green density, as observed for CG (Fig. 5). Because differences in shrinkage behavior can be compensated for in the design of the printed parts in additive manufacturing, these small variations in shrinkage factors do not affect the performance of the feedstocks for the LSD-print process.

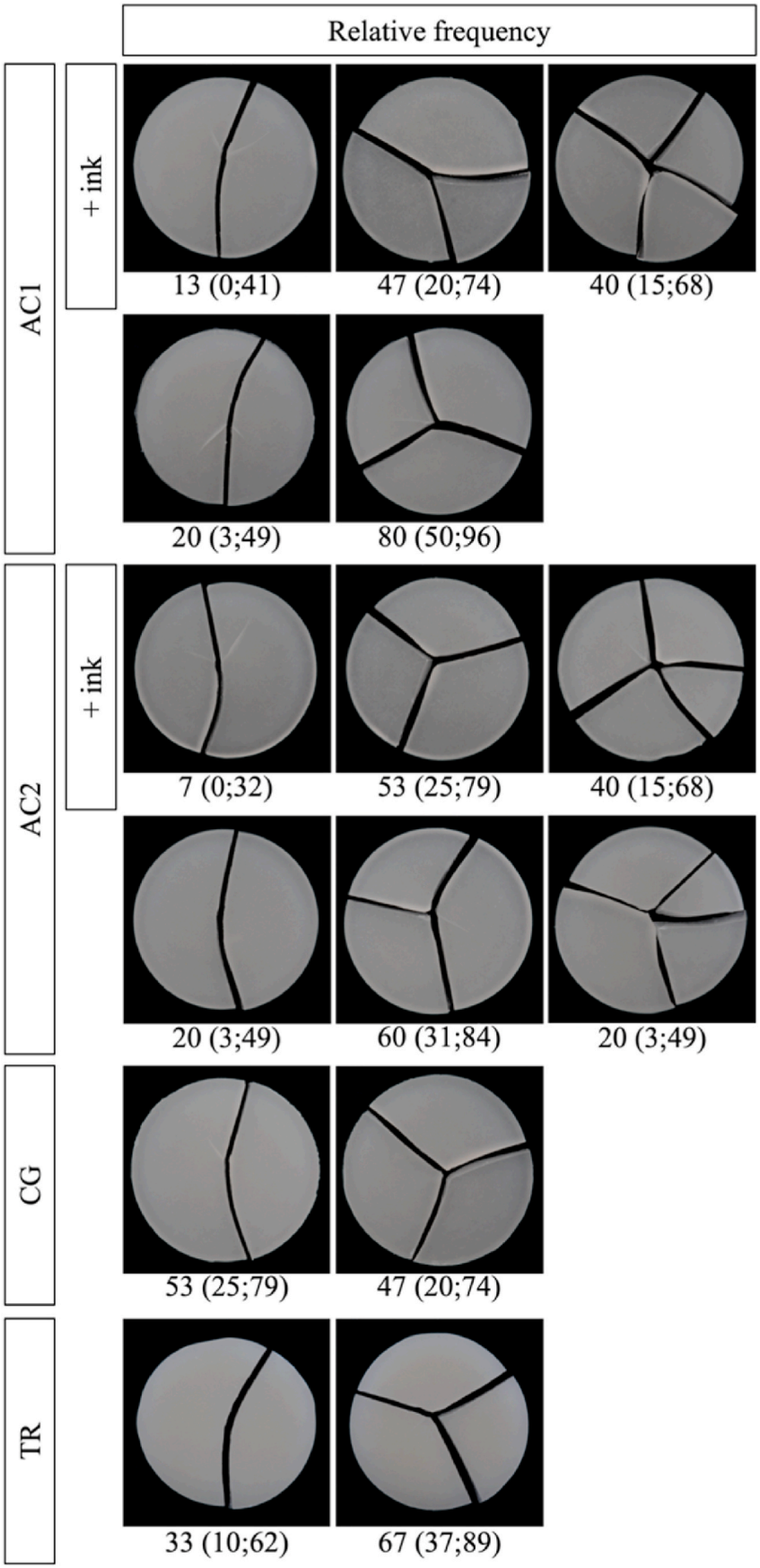

Fig. 7. Relative frequency of fracture types classified into two, three, and four fragments.

4.2. Discussion of null hypothesis (2): influence of ink

In the green state, the relative increase in FS was almost 20 times for both AC1+ink and AC2+ink compared with AC1 and AC2, respectively. This significant increase can be attributed to the addition of ink, which, after thermal processing, forms a strong covalently cross-linked network holding the ceramic particles, resulting in a stable green body.

From the perspective of the application of feedstocks in the LSD-print process, the green strength with ink is important for handling the as-printed parts and to extract them from the surrounding powder at the end of the printing process. A biaxial strength of several MPa (approx. 8 MPa for AC1+ink and 5 MPa for AC2+ink) is sufficient for easy handling (Diener et al., 2023; Gilmer et al., 2021).

In the fired state, the use of ink led to a slight decrease in fracture toughness for both AC1+ink and AC2+ink (compared with AC1 and AC2, respectively). In particular, the AC2+ink group had the lowest value of K_{IC} of all groups at 0.86 ± 0.06 MPa·$m^{0.5}$. These results suggest that the use of the phenolic resin ink tested in this study had a small negative effect on the fracture toughness of the fired material. This effect will have to be investigated in more detail in future studies dedicated to the LSD-printing process to determine whether the same effect is also observed in LSD-printed specimens.

4.3. Discussion of null hypothesis (3): comparison to TR

The results of this investigation indicate that most physical properties of the slip-cast groups in the fired state were comparable with those of the commercial target reference (TR group, Table 3). Significant differences in FS and fracture toughness were found in the pairwise comparisons between TR and some of the slip-cast groups; however, this conclusion cannot be statistically generalized to all slip-cast groups. Nevertheless, the mean values of TR for fracture strength, fracture toughness, Martens parameters, and Weibull modulus were the highest of all groups. A significant difference was also found for the absolute density, which was significantly higher for TR than for all slip-cast groups. The density of TR was comparable with that reported previously (Thompson et al., 1996). These observations suggest some general differences between the microstructures of TR and slip-cast groups in the fired state.

Such microstructural differences can be identified in Fig. 4 and in Fig. 5, which show a lower crystalline fraction in the slip-cast groups than in the TR.

The higher absolute density probably arises from the higher crystalline fraction in TR because feldspathic crystal phases have a higher density than their parent glass (Taylor and Brown Jr, 1979). The commercially available VITA Mark II material (i.e., TR in this investigation) is composed of nepheline ($Na_3KAl_4Si_4O_{16}$), sanidine ($KAlSi_3O_8$), and anorthoclase ($(Na,K)AlSi_3O_8$) crystalline phases in a glassy matrix (Yin et al., 2006). Nepheline is readily dissolved in strong inorganic acids (Shand, 1939); thus, the images of the etched microstructures in Fig. 4 can be interpreted as nepheline being the deeply etched phase, with sanidine in the foreground as the second crystal phase with a lower etching rate than the glass. The EDX analysis in Fig. 5 qualitatively confirms that the same crystalline phases can be assigned to the microstructure of the slip-cast material in the fired state.

Although the reason for the decrease in the crystalline fraction in the slip-cast material compared with TR has not been investigated thoroughly, it seems likely related to the different thermal history of the material. Because TR is a commercial product and its thermal treatment is unknown, further studies are necessary to understand the effect of the thermal history on the crystallization of the material. From the current work, however, it can be stated that the observed differences in bulk density between the slip-cast groups and TR are unlikely to be related to any negative effect the additives have on the densification mechanisms. The relative density of all groups, including TR, was found to be in the same range, indicating that all specimens could be fired to obtain a dense microstructure (>99% relative density).

The observed similarities in mechanical properties between slip-cast groups (in the fired state) and TR are a result of the similarity between the relative density, crystallized phases, and distribution of defects. Nevertheless, small differences in the fracture toughness can be explained by the observed differences in the crystalline fraction of the material. A higher crystalline content with a homogeneous distribution of crystals of different sizes has been associated with a higher fracture toughness owing to crack-deflection (Quinn et al., 2003) and because indentation cracks in a silicate glass-ceramic are deflected away from the embedded crystals and favor the glassy matrix for propagation (Morena et al., 1986; Quinn et al., 2003). Similarly, a higher Martens hardness can also be correlated with a higher crystalline fraction.

Despite the observed microstructural differences, slip-cast specimens from groups AC1/AC1+ink and AC2/AC2+ink had a flexural strength in the same range as common feldspathic glass-ceramic CAD/CAM blocks, which is typically approximately 100 MPa (Bindl et al., 2003; Coldea et al., 2015; Sen and Us, 2018; Thompson et al., 1996). These values vary depending on the composition, production process, specimen preparation, and testing method (Fischer et al., 2008; Wendler et al., 2017). For this reason, it can be stated that AC1 and AC2 are appropriate feedstocks for the manufacturing of restorations with a clinical application for low load-bearing anterior but high esthetic applications (e.g., veneers) (2019; Saint-Jean, 2014). Future studies should investigate the Poisson ratio for all tested groups, especially in the fired state, to calculate the flexural strength and Martens parameter more accurately. Börger et al. (2004) reported that a deviation of υ in the range of ±0.05 leads to an error of ±5% in the calculation of the biaxial strength. However, the current work focused on the relative comparison between groups of similar materials, for which only small variations of υ (between groups of fired specimens and between groups of green specimens) are expected.

5. Conclusions

Based on the findings of this in vitro study, the following conclusions were drawn.

1. The use of additives in the formulation of slurry feedstock results in a decrease in green density for slip-cast specimens. Binders and plasticizers, however, increase the green stability of slip-cast materials and are essential components of feedstock composition. Furthermore, the use of PVA (feedstock AC1) and PSS + PEG (feedstock AC2) as additives had no negative impact on the material properties in the fired state compared with a control group (CG) without additives.
2. The addition of ink to AC1 and AC2 resulted in a large increase (up to 20 times) in the fracture strength of the slip-cast material in the green state. Considering the application perspective in the LSD-print additive manufacturing process, this result suggests that a green strength of 5–8 MPa can be obtained for the as-printed specimens, sufficient for easy handling. Notably, the use of the ink tested in this study (phenolic resin) had a small negative effect on the fracture toughness of the fired material. This effect needs to be investigated in more detail in future studies.
3. The fracture toughness of slip-cast specimens of the experimental feedstock compositions was slightly lower than that of the target reference (TR) manufactured from commercially available CAD/CAM blocks with the same nominal composition. The main reason for this difference is likely a lower crystalline fraction in the slip-cast specimens after firing compared with TR. By optimizing the firing parameters, a more similar microstructure may be generated in the future.
4. Overall, the results of the study suggest that both AC1 and AC2 are promising candidate feedstocks for LSD-print in combination with the tested ink.

5. The tested values for FS in the fired state were in accordance with the requirements for anterior monolithic single-tooth crowns, veneers, inlays or onlays (class 1a) (2019).

Funding

This work was supported by research grant KK5056001AG0 (AiF Projekt GmbH, Berlin, Germany, ZIM-Kooperationsprojekte, Projektträger des BMWK).

CRediT authorship contribution statement

Moritz Hoffmann: Writing – review & editing, Writing – original draft, Visualization, Validation, Resources, Project administration, Methodology, Investigation, Formal analysis, Data curation, Conceptualization. **Bogna Stawarczyk:** Writing – review & editing, Project administration, Funding acquisition, Conceptualization. **Jens Günster:** Writing – review & editing, Project administration, Funding acquisition, Conceptualization. **Andrea Zocca:** Writing – review & editing, Writing – original draft, Visualization, Validation, Project administration, Methodology, Investigation, Formal analysis, Data curation, Conceptualization.

Declaration of competing interest

The authors declare that they have no known competing financial interests or personal relationships that could have appeared to influence the work reported in this paper.

Data availability

Data will be made available on request.

Acknowledgements

This work was supported by research program KK5056001AG0 (AiF Projekt GmbH, Berlin, Germany, ZIM-Kooperationsprojekte, Projektträger des BMWK). The authors would like to thank VITA Zahnfabrik for material and r2 dei ex machina for shrinking analyzing software support of the investigation.

References

Albakry, M., Guazzato, M., Swain, M.V., 2003. Biaxial flexural strength, elastic moduli, and x-ray diffraction characterization of three pressable all-ceramic materials. J. Prosthet. Dent 89, 374–380.
Bajraktarova-Valjakova, E., Korunoska-Stevkovska, V., Kapusevska, B., Gigovski, N., Bajraktarova-Misevska, C., Grozdanov, A., 2018. Contemporary dental ceramic materials, a review: chemical composition, physical and mechanical properties, indications for use. Maced J Medical Sci 6, 1742.
Barazanchi, A., Li, K.C., Al-Amleh, B., Lyons, K., Waddell, J.N., 2017. Additive technology: update on current materials and applications in dentistry. J. Prosthodont. 26, 156–163.
Bindl, A., Luthy, H., Mormann, W.H., 2003. Fracture load of CAD/CAM-generated slot-inlay FPDs. Int. J. Prosthodont. (IJP) 16, 653–660.
Börger, A., Supancic, P., Danzer, R., 2004. The ball on three balls test for strength testing of brittle discs: Part II: analysis of possible errors in the strength determination. J. Eur. Ceram. Soc. 24, 2917–2928.
Branco, A.C., Colaço, R., Figueiredo-Pina, C.G., Serro, A.C., 2023. Recent Advances on 3D-printed zirconia-based dental materials: a review. Materials 16, 1860.
Butikofer, L., Stawarczyk, B., Roos, M., 2015. Two regression methods for estimation of a two-parameter Weibull distribution for reliability of dental materials. Dent. Mater. 31, e33–e50.
Carter, C.B., Norton, M.G., 2007. Ceramic Materials: Science and Engineering. Springer, p. 716.
Chiu, R.C., Garino, T., Cima, M., 1993. Drying of granular ceramic films: I, effect of processing variables on cracking behavior. J. Am. Ceram. Soc. 76, 2257–2264.
Cima, M., Oilveira, M., Wang, H., Sachs, E., Holman, R., 2001. Slurry-based 3DP and fine ceramic components. In: 2001 International Solid Freeform Fabrication Symposium.
Coldea, A., Fischer, J., Swain, M.V., Thiel, N., 2015. Damage tolerance of indirect restorative materials (including PICN) after simulated bur adjustments. Dent. Mater. 31, 684–694.
Conrad, H.J., Seong, W.J., Pesun, I.J., 2007. Current ceramic materials and systems with clinical recommendations: a systematic review. J. Prosthet. Dent 98, 389–404.
Daher, R., Ardu, S., di Bella, E., Krejci, I., Duc, O., 2022. Efficiency of 3D-printed composite resin restorations compared with subtractive materials: evaluation of fatigue behavior, cost, and time of production. J. Prosthet. Dent. https://doi.org/10.1016/j.prosdent.2022.08.001.
Diener, S., Schubert, H., Günster, J., Zocca, A., 2023. Ink development for the additive manufacturing of strong green parts by layerwise slurry deposition (LSD-print). J. Am. Ceram. Soc. 106, 2752–2763.
Fischer, J., Stawarczyk, B., Hammerle, C.H., 2008. Flexural strength of veneering ceramics for zirconia. J. Dent. 36, 316–321.
Galante, R., Figueiredo-Pina, C.G., Serro, A.P., 2019. Additive manufacturing of ceramics for dental applications: a review. Dent. Mater. 35, 825–846.
Gilmer, D.B., Han, L., Lehmann, M.L., Siddel, D.H., Yang, G., Chowdhury, A.U., Doughty, B., Elliott, A.M., Saito, T., 2021. Additive manufacturing of strong silica sand structures enabled by polyethyleneimine binder. Nat. Commun. 12, 5144.
Greaves, G.N., Greer, A.L., Lakes, R.S., Rouxel, T., 2011. Poisson's ratio and modern materials. Nat. Mater. 10, 823–837.
Hampton, J.H.D., Savage, S.B., Drew, R.A., 1988. Experimental analysis and modeling of slip casting. J. Am. Ceram. Soc. 71, 1040–1045.
Hotza, D., Greil, P., 1995. Aqueous tape casting of ceramic powders. Mater Sci Eng C 202, 206–217.
Ioannidis, A., Bomze, D., Hammerle, C.H.F., Husler, J., Birrer, O., Muhlemann, S., 2020. Load-bearing capacity of CAD/CAM 3D-printed zirconia, CAD/CAM milled zirconia, and heat-pressed lithium disilicate ultra-thin occlusal veneers on molars. Dent. Mater. 36, e109–e116.
Kelly, J.R., Benetti, P., 2011. Ceramic materials in dentistry: historical evolution and current practice. Aust. Dent. J. 56, 84–96.
Kelly, J.R., Nishimura, I., Campbell, S.D., 1996. Ceramics in dentistry: historical roots and current perspectives. J. Prosthet. Dent 75, 18–32.
Kim, D.-J., Park, I.-S., Lee, M.-H., 2005. Tensile strength of aqueous-based alumina tapes using a PVP–PVA–gelatin cobinder. Ceram. Int. 31, 577–581.
Lerner, H., Nagy, K., Pranno, N., Zarone, F., Admakin, O., Mangano, F., 2021. Trueness and precision of 3D-printed versus milled monolithic zirconia crowns: an in vitro study. J. Dent. 113, 103792.
Lima, P., Zocca, A., Acchar, W., Günster, J., 2018. 3D printing of porcelain by layerwise slurry deposition. J. Eur. Ceram. Soc. 38, 3395–3400.
Lüchtenborg, J., Willems, E., Zhang, F., Wesemann, C., Weiss, F., Nold, J., Sun, J., Sandra, F., Bai, J., Reveron, H., 2022. Accuracy of additively manufactured zirconia four-unit fixed dental prostheses fabricated by stereolithography, digital light processing and material jetting compared with subtractive manufacturing. Dent. Mater. 38, 1459–1469.
Morena, R., Lockwood, P.E., Fairhurst, C.W., 1986. Fracture toughness of commercial dental porcelains. Dent. Mater. 2, 58–62.
Park, J.-S., Lim, Y.-J., Kim, B., Kim, M.-J., Kwon, H.-B., 2020. Clinical evaluation of time efficiency and fit accuracy of lithium disilicate single crowns between conventional and digital impression. Materials 13, 5467.
Quinn, J.B., Sundar, V., Lloyd, I.K., 2003. Influence of microstructure and chemistry on the fracture toughness of dental ceramics. Dent. Mater. 19, 603–611.
Rodrigues, I., Guedes, M., Olhero, S., Chefdor, A., Branco, A.C., Leite, M., Serro, A.P., Figueiredo-Pina, C.G., 2020. Development of free binder zirconia-based pastes for the production of T dental pieces by robocasting. J. Manuf. Process. 57, 1–9.
Sadowsky, S.J., 2006. An overview of treatment considerations for esthetic restorations: a review of the literature. J. Prosthet. Dent 96, 433–442.
Saint-Jean, S.J., 2014. Dental glasses and glass-ceramics. J Adv Ceram 12, 255–277.
Sen, N., Us, Y.O., 2018. Mechanical and optical properties of monolithic CAD-CAM restorative materials. J. Prosthet. Dent 119, 593–599.
Shand, S.J., 1939. On the staining of feldspathoids, and on zonal structure in nepheline. Am. Mineral. 24, 508–513.
Taylor, M., Brown Jr, G.E., 1979. Structure of mineral glasses - I. The feldspar glasses NaAlSi3O8, KAlSi3O8, CaAl2Si2O8. Geochim Cosmochim Acta 43, 61–75.
Thompson, J.Y., Bayne, S.C., Heymann, H.O., 1996. Mechanical properties of a new mica-based machinable glass ceramic for CAD/CAM restorations. J. Prosthet. Dent 76, 619–623.
Tomas, J., Kleinschmidt, S., 2009. Improvement of flowability of fine cohesive powders by flow additives. Chem. Eng. Technol. 32, 1470–1483.
Turkyilmaz, I., Wilkins, G.N., Varvara, G., 2021. Tooth preparation, digital design and milling process considerations for CAD/CAM crowns: understanding the transition from analog to digital workflow. J. Dent. Sci. 16, 1312.
Uhland, S.A., Holman, R.K., Morissette, S., Cima, M.J., Sachs, E.M., 2001. Strength of green ceramics with low binder content. J. Am. Ceram. Soc. 84, 2809–2818.
Unkovskiy, A., Beuer, F., Metin, D.S., Bomze, D., Hey, J., Schmidt, F., 2022. Additive manufacturing of lithium disilicate with the LCM process for classic and non-prep veneers: preliminary technical and clinical case experience. Materials 15, 6034.
Wang, W., Sun, J., 2021. Dimensional accuracy and clinical adaptation of ceramic crowns fabricated with the stereolithography technique. J. Prosthet. Dent 125, 657–663.
Wang, W., Yu, H., Liu, Y., Jiang, X., Gao, B., 2019. Trueness analysis of zirconia crowns fabricated with 3-dimensional printing. J. Prosthet. Dent 121, 285–291.
Wendler, M., Belli, R., Petschelt, A., Mevec, D., Harrer, W., Lube, T., Danzer, R., Lohbauer, U., 2017. Chairside CAD/CAM materials. Part 2: flexural strength testing. Dent. Mater. 33, 99–109.

Yin, L., Song, X., Qu, S., Han, Y., Wang, H., 2006. Surface integrity and removal mechanism in simulated dental finishing of a feldspathic porcelain. J. Biomed. Mater. Res. Part B Appl Biomater 79, 365–378.
Zocca, A., Lima, P., Günster, J., 2017. LSD-based 3D printing of alumina ceramics. J. Ceram. Sci. Technol. 8, 141–148.
Zocca, A., Lima, P., Diener, S., Katsikis, N., Günster, J., 2019. Additive manufacturing of SiSiC by layerwise slurry deposition and binder jetting (LSD-print). J. Eur. Ceram. Soc. 39, 3527–3533.